

A quasi-physical family of gravity-wave templates for precessing binaries of spinning compact objects: II. Application to double-spin precessing binaries

Alessandra Buonanno,¹ Yanbei Chen,² Yi Pan,² and Michele Vallisneri³

¹*Groupe de Gravitation et Cosmologie (GReCO),*

Institut d'Astrophysique de Paris (CNRS), 98^{bis} Boulevard Arago, 75014 Paris, France

²*Theoretical Astrophysics and Relativity, California Institute of Technology, Pasadena, CA 91125*

³*Jet Propulsion Laboratory, California Institute of Technology, Pasadena, CA 91109*

(Dated: May 11, 2004)

The gravitational waveforms emitted during the adiabatic inspiral of precessing binaries with two spinning compact bodies of comparable masses, evaluated within the post-Newtonian approximation, can be reproduced rather accurately by the waveforms obtained by setting one of the two spins to zero, at least for the purpose of detection by ground-based gravitational-wave interferometers. Here we propose to use this quasi-physical family of single-spin templates to search for the signals emitted by double-spin precessing binaries, and we find that its signal-matching performance is satisfactory for source masses $(m_1, m_2) \in [3, 15]M_\odot \times [3, 15]M_\odot$. For this mass range, using the LIGO-I design sensitivity, we estimate that the number of templates required to yield a minimum match of 0.97 is $\sim 320,000$. We discuss also the accuracy to which the single-spin template family can be used to estimate the parameters of the original double-spin precessing binaries.

PACS numbers: 04.30.Db, 04.25.Nx, 04.80.Nn, 95.55.Ym

I. INTRODUCTION

An international network of long-baseline laser-interferometric gravitational-wave detectors, consisting of the Laser-Interferometer Gravitational-wave Observatory (LIGO) [1], of VIRGO [2], of GEO 600 [3] and of TAMA 300 [4], has by now begun science operations. VIRGO is in its commissioning phase, while LIGO has already completed three science runs (S1 on August–September 2002 [5], S2 on February–April 2003, and S3 on October 2003–January 2004; S1 and S3 were in coincidence with GEO 600) with increasing sensitivity and stability. The analysis of S1 data has been completed, yielding new upper limits on event rates for various classes of astrophysical sources [6]; the data from S2 and S3 are still being analyzed. LIGO is expected to reach its full design sensitivity in 2005.

Compact binaries consisting of black holes (BHs) and neutron stars (NSs) are among the most promising [7] and best understood sources for such gravitational-wave (GW) interferometers, which can observe the waves emitted by the binaries in the adiabatic-inspiral regime, where post-Newtonian (PN) calculations [8, 9, 10, 11, 12, 13, 14, 15, 16, 17] are appropriate to describe the orbital dynamics and predict the gravitational waveforms.

Very little is known about the statistical distributions of BH spins in compact binaries: the spins could be large, and they need not be aligned with the orbital angular momentum. When this is the case, spin-orbit and spin-spin interactions can cause the rapid precession of the orbital plane of the binary, and thus significant modulations of the emitted GWs, as it was shown by Apostolatos, Cutler, Sussman and Thorne (ACST) [18], and later by Apostolatos [19]. These modulational effects should be included in the theoretical waveform models (templates) used in matched-filtering GW searches. However, using

template banks parametrized by all the relevant physical parameters (the masses, the spins, the angles that describe the relative orientations of detector and binary, and the direction of propagation of GWs to the detector) would make such searches extremely computationally intensive.

One possibility to reduce the computational cost is the adoption of smaller *detection template families* (DTF), which capture the essential features of the true waveforms, but depend on a smaller number of parameters. A DTF for precessing binaries was first proposed by Apostolatos [20, 21], building on the analysis of precessional dynamics of Refs. [18, 19]. However, according to Apostolatos' own estimates and to Grandclément, Kalogera and Vecchio's later tests [22], the computational resources required by the Apostolatos DTF are still prohibitive, and its signal-matching performance is unsatisfactory. The latter is improved in a modified version of the DTF [23, 24], which adds δ -like *spikes* in the waveform phase.

Buonanno, Chen and Vallisneri [25, henceforth BCV2] investigated the dynamics of precession further, and proposed a new convention to write the dominant quadrupolar contribution to GW emission. In this convention, the oscillatory effects of precession are isolated in the evolution of the GW polarization tensors, which are combined with the detector's *antenna patterns* to yield its response. As a result, the response can be written as the product of a carrier signal and a modulational correction, which can be handled using an extension of Apostolatos' treatment of precessional effects. BCV2 cast these waveforms into a mathematical structure that allows searching automatically and economically over all the parameters related to precessional modulations, except for a single parameter that describes the timescale of modulation. The BCV2 DTF has reasonable computational requirements

and good signal-matching capabilities. However, especially for binaries with high, comparable masses, it has the shortcoming that a large number of unphysical waveforms are automatically included in GW searches (albeit at no extra computational cost), increasing the probability of false alarms triggered by noise. [This shortcoming is unfortunately but unavoidably characteristic of DTFs, which replace a description in terms of physical source parameters by one in terms of phenomenological signal parameters.]

This paper is the second in a series (begun with Ref. [26]) written to investigate the possibility of searching for precessing binaries using a *physical* family of signal templates (a PTF) computed from the PN equations of motion. Although at first sight the number of physical parameters necessary to describe a waveform is large, we were able to reduce the effective dimensionality of the template family using the insight developed in the construction of DTFs. As mentioned above, BCV2 [25, Sec. VI D] established that it is possible to search easily over most of the parameters related to the kinematics of precession (such as the orientation of the detector and of the binary as a whole, the direction of GW propagation, and the initial orbital phase). In effect, these *extrinsic* parameters can be incorporated in the detection statistic, while single “templates” [27] remain functions only of the masses of the binary components, of the magnitudes of their spins, and of the relative angles between the spins and the orbital angular momentum at a fiducial frequency. Under the assumption of circular adiabatic inspiral [28], seven such *intrinsic* parameters are needed for a generic binary where both spins are important (henceforth, a *double-spin binary*); four are needed for a binary where only one body has significant spin (henceforth, a *single-spin binary*). (See Sec. II for the distinction between extrinsic and intrinsic parameters.)

In Ref. [26], we demonstrated the feasibility of a PTF search for single-spin binaries: we described a two-stage algorithm to search over the extrinsic parameters (the first stage emphasizes computational efficiency, but retains some unphysical waveforms; the second stage, applied only to first-stage triggers, restricts the possible search outcomes to physical configurations). Using this algorithm, we tested a four-parameter PTF for binaries with $(m_1, m_2) \in [7M_\odot, 12M_\odot] \times [1M_\odot, 3M_\odot]$, where the assumption of a single significant spin is justified. We found that $\sim 76,000$ templates are required for a search in this mass range, for a minimal match of 0.97 (see Sec. II for a definition of minimal match); under the assumption of Gaussian, stationary noise, we also found that the detection threshold required for a given false-alarm probability is lower in the PTF search than in a DTF search with the same number of intrinsic parameters.

In this paper we examine PTF searches for the more general class of double-spin binaries. Although in this case we have seven intrinsic parameters, they are not all essential in determining the waveforms. This is strictly true in two limits. First, as it was realized by ACST [18],

if the two binary masses are equal, and if spin-spin interactions are ignored, the same orbital evolution can be replicated by giving the total spin to one of the objects. Indeed, for the mass ranges of interest to ground-based interferometers, spin-spin effects contribute mildly to the binding energy and to the PN GW flux, even close to the last stable orbit. Second, if the mass ratio $\eta = m_1 m_2 / (m_1 + m_2)^2$ is very low (as it was assumed in Ref. [26]), the spin of the less massive object can be ignored. In addition, as investigated by BCV2 (and less systematically by Kidder [10]), the dynamics of double-spin binaries with generic mass ratios show features similar to those described by ACST for single-spin binaries.

These arguments have led us to conjecture that single-spin waveforms may always be sufficient to approximate double-spin waveforms, at least for the purpose of GW searches with ground-based interferometers. Since the single-spin parameters that best reproduce a given double-spin signal might not be in the physical range for a true single-spin binary (for instance, because the spin of one of two objects must do the work of two, it might have to exceed the maximal spin allowed for BHs), the single-spin family should be called *quasi-physical*, but we shall continue to use “PTF” loosely. In the rest of this paper, we present evidence that our conjecture is correct for the mass range $(m_1, m_2) \in [3M_\odot, 15M_\odot] \times [3M_\odot, 15M_\odot]$, and we examine the computational requirements and the parameter-estimation performance of a single-spin PTF search for double-spin binaries in this mass range.

This paper is organized as follows. In Sec. II, we provide a short glossary for the notions and quantities of matched-filtering GW searches (some standard, some developed in Ref. [26]) that are needed later. In Sec. III A, we review the adiabatic PN dynamics of double-spin binaries; in Sec. III B, we describe our family of quasi-physical single-spin templates, and we evaluate their signal-matching capabilities against double-spin binaries with maximal spins (where precessional effects are expected to be strongest); in Sec. III C, we study the robustness of adiabatic PN waveforms for binaries with high, comparable masses; in Sec. III D, we discuss some features of double-spin binary dynamics that help to explain the good signal-matching performance of single-spin templates. In Sec. IV, we estimate the number of templates required in a single-spin PTF search in our mass range of interest. In Sec. V, we investigate the extraction of the physical parameters of the double-spin binary using single-spin templates. Last, in Sec. VI we summarize our main conclusions.

II. A GLOSSARY OF MATCHED-FILTERING GW DETECTION

In this paper we adopt the standard formalism of matched-filtering GW detection, as summarized in Ref. [17] (which includes an extensive bibliography), and as extended in Ref. [26] to a special treatment of extrin-

sic and intrinsic parameters. Here we provide a glossary of the notions used in this paper, with pointers to their definitions in Refs. [17, 26].

Templates $h(\lambda^A)$: Theoretical models of GW signals, parametrized by one or more *template parameters* λ^A . A *continuous template family* $\{h(\lambda^A)\}$ defines a smooth submanifold in signal space.

Noise inner product $\langle f, g \rangle$: Eq. (1) of Ref. [17]. A measure of the closeness of two signal, as given by a correlation product weighted by the power spectral density of noise; throughout this paper we adopt the LIGO-I one-sided noise power spectral density S_n given by Eq. (28) of Ref. [17]. A *normalized* template $\hat{h}(\lambda^A)$ has $\langle \hat{h}(\lambda^A), \hat{h}(\lambda^A) \rangle = 1$.

Match: Inner product of two normalized signals. The *mismatch* is one minus the match.

Overlap $\rho(s, h(\lambda^A))$: Inner product of a signal s with the normalized template $\hat{h}(\lambda^A)$.

Detection statistic: Figure of merit compared with a *detection threshold* to decide whether the signal modeled by a template $h(\lambda^A)$ is present in the detector output o . For Gaussian, stationary noise, the overlap $\rho(o, h(\lambda^A))$ is the *optimal* statistic that minimizes the probability of false dismissal for a given probability of false alarm (set by the detection threshold). In this context ρ is also known as the *signal-to-noise ratio* (S/N) of the detector output after filtering by the template $\hat{h}(\lambda^A)$. The corresponding detection statistic for an entire template family $\{h(\lambda^A)\}$ is the maximized overlap $\max_{\lambda^A} \rho(o, h(\lambda^A))$.

Fitting factor FF [29]: Eq. (20) of Ref. [17]. Match between a template in a *target* family (representing actual physical signals) and a template in a *search* family, *maximized over all the parameters of the search family*. The FF (a value between 0 and 1) characterizes the effectualness of the search family in reproducing signals modeled by the target family: using an imperfect family means that only a fraction FF of the available S/N is recovered, reducing the number of true events that pass the detection threshold. The maximized match induces a (many-to-one) map between the space of target parameters and the space of search parameters (see Sec. V on the systematic errors in parameter estimation induced by this map).

Extrinsic (Θ^μ) and *intrinsic* (X^i) *template parameters*: Extrinsic parameters are those over which ρ can be maximized efficiently, without recomputing full search templates for each set of extrinsic parameters under consideration (but perhaps using a small number of sub-templates) [30]. By contrast, maximizing ρ over the intrinsic parameters requires computing a full template for each different set of intrinsic parameters in the search range. Searches for signals modeled by a template family $\{h(\lambda^A) \equiv h(X^i, \Theta^\mu)\}$ are usually implemented by obtaining $\max_{\Theta^\mu} \rho$ for each template in a discrete bank $\{h(X_{(k)}^i, \Theta^\mu)\}$, laid down only along the intrinsic-parameter directions.

Minimum match MM and *mismatch metric* [31]: Eqs.

(21)–(24) of Ref. [17]. The spacing of discrete search banks is chosen so that at most a fraction MM is lost from the S/N that would be obtained with a continuous search bank; the corresponding loss in detection rate, for the same detection threshold, is a fraction MM^3 . The choice of the spacing is helped by considering the (full) *mismatch metric* g_{AB} , which serves as a local quadratic expansion of the mismatch over all the search parameters. An approximation to the number of templates needed to achieve a given MM , computed using the metric, is given by Eq. (25) of Ref. [17].

Projected metric: Eqs. (65) and (72) of Ref. [26]. Given that the search template bank has no extension along the extrinsic-parameter directions, it is useful to consider a projected metric g_{ij}^{proj} that approximates the mismatch *already minimized over the extrinsic search parameters*. This g_{ij}^{proj} is still a function of the intrinsic and *extrinsic target* parameters. The *average projected metric* $\overline{g_{ij}^{\text{proj}}}$ (Eq. (75) of Ref. [26]) is a weighted average over the extrinsic target parameters, which can be used to estimate the number of templates needed to achieve a given reduction in detection rate, for a uniform distribution of target extrinsic parameters (this reduction is proportional to \overline{MM}^3 , where \overline{MM} is the *average minimum match*).

Reduced search parameter space and reduction curves [26, 32]: It can happen that the variety of waveforms spanned by an n -dimensional (search) template family is approximated with very high FF by an $(n - k)$ -dimensional subset of the family (a *reduced family*). This circumstance is signaled locally in the mismatch metric by the presence of k *quasi-null directions* (i.e., eigenvectors with very small eigenvalues). The integral curves of these directions (the *reduction curves*) correspond to sets of templates with very high match within the set, and map a reduced family into another. In this case, it is advantageous to derive the discrete search bank from a reduced family: ideally, one would reparametrize the full family using k parameters that run along the reduction curves, and then discard those parameters before laying down templates. See Ref. [26] for a thorough discussion.

III. SINGLE-SPIN TEMPLATE FAMILY TO MATCH DOUBLE-SPIN PRECESSING BINARIES

This section contains the main results of this paper. In Sec. III A we describe the PN equations for the circular adiabatic inspiral of a double-spin binary; this *target model* is used throughout this paper to represent physical signals. In Sec. III B we describe our proposed single-spin *search template family*, and we evaluate its effectualness (which is excellent) in approximating the target waveforms. In Sec. III C we compare single-spin signals obtained at different PN orders, to argue that the circular adiabatic model of inspirals used in this paper gives robust predictions for the actual physical wave-

forms. Last, in Sec. IIID we study the precessional dynamics of double-spin binaries to understand which of its features can be represented accurately by single-spin systems, and which cannot.

A. Target model: double-spin precessing binaries

Post-Newtonian calculations provide the following set of equations describing the adiabatic evolution of double-

spin precessing binaries. The first derivative of the orbital (angular) frequency, up to 3.5PN order [33] reads [8, 9, 10, 11, 12, 13, 14, 15, 25]:

$$\frac{\dot{\omega}}{\omega^2} = \frac{96}{5} \eta (M\omega)^{5/3} (1 + \mathcal{P}_{1\text{PN}} + \mathcal{P}_{1.5\text{PN}} + \mathcal{P}_{2\text{PN}} + \mathcal{P}_{2.5\text{PN}} + \mathcal{P}_{3\text{PN}} + \mathcal{P}_{3.5\text{PN}}), \quad (1)$$

where

$$\mathcal{P}_{1\text{PN}} = -\frac{743 + 924\eta}{336} (M\omega)^{2/3}, \quad (2)$$

$$\mathcal{P}_{1.5\text{PN}} = -\left(\frac{1}{12} \sum_{i=1,2} \left[\chi_i (\hat{\mathbf{L}}_N \cdot \hat{\mathbf{S}}_i) \left(113 \frac{m_i^2}{M^2} + 75\eta \right) \right] - 4\pi\right) (M\omega), \quad (3)$$

$$\mathcal{P}_{2\text{PN}} = \left\{ \left(\frac{34103}{18144} + \frac{13661}{2016} \eta + \frac{59}{18} \eta^2 \right) - \frac{1}{48} \eta \chi_1 \chi_2 \left[247 (\hat{\mathbf{S}}_1 \cdot \hat{\mathbf{S}}_2) - 721 (\hat{\mathbf{L}}_N \cdot \hat{\mathbf{S}}_1) (\hat{\mathbf{L}}_N \cdot \hat{\mathbf{S}}_2) \right] \right\} (M\omega)^{4/3}, \quad (4)$$

$$\mathcal{P}_{2.5\text{PN}} = -\frac{1}{672} (4159 + 14532\eta) \pi (M\omega)^{5/3}, \quad (5)$$

$$\begin{aligned} \mathcal{P}_{3\text{PN}} = & \left[\left(\frac{16447322263}{139708800} - \frac{1712}{105} \gamma_E + \frac{16}{3} \pi^2 \right) + \left(-\frac{273811877}{1088640} + \frac{451}{48} \pi^2 - \frac{88}{3} \hat{\theta} \right) \eta \right. \\ & \left. + \frac{541}{896} \eta^2 - \frac{5605}{2592} \eta^3 - \frac{856}{105} \log \left[16(M\omega)^{2/3} \right] \right] (M\omega)^2, \end{aligned} \quad (6)$$

$$\mathcal{P}_{3.5\text{PN}} = \left(-\frac{4415}{4032} + \frac{661775}{12096} \eta + \frac{149789}{3024} \eta^2 \right) \pi (M\omega)^{7/3}. \quad (7)$$

Here, m_1 and m_2 are the masses of the two bodies, with $m_1 \geq m_2$; $M = m_1 + m_2$ is the total mass, and $\eta = m_1 m_2 / M^2$ is the symmetric mass ratio; $\mathbf{L}_N = \mu \mathbf{x} \times \mathbf{v}$ (with $\mu = m_1 m_2 / M$) is the Newtonian angular momentum (with \mathbf{x} and \mathbf{v} the two-body center-of-mass radial separation and relative velocity), and $\hat{\mathbf{L}}_N = \mathbf{L}_N / |\mathbf{L}_N|$; $\mathbf{S}_1 = \chi_1 m_1^2 \hat{\mathbf{S}}_1$ and $\mathbf{S}_2 = \chi_2 m_2^2 \hat{\mathbf{S}}_2$ are the spins of the two bodies (with $\hat{\mathbf{S}}_{1,2}$ unit vectors, and $0 < \chi_{1,2} < 1$ for BHs); $\gamma_E = 0.577\dots$ is Euler's constant; last, $\hat{\theta} =$

$\theta + 1987/1320 + 7\omega_s/11$ (with θ an unknown arbitrary parameter that enters the GW flux at 3PN order [13], and $\omega_s = 0$ [12, 14, 15]).

In Eq. (1) we did not include the quadrupole-monopole terms [34], because we have already shown (see Sec. III E of Ref. [26]) that those terms do not significantly affect matches once these are maximized on binary parameters. The precession equations for the spins read [10,18]

$$\dot{\mathbf{S}}_1 = \frac{(M\omega)^2}{2M} \left\{ \eta (M\omega)^{-1/3} \left(4 + 3 \frac{m_2}{m_1} \right) \hat{\mathbf{L}}_N + \frac{1}{M^2} \left[\mathbf{S}_2 - 3(\mathbf{S}_2 \cdot \hat{\mathbf{L}}_N) \hat{\mathbf{L}}_N \right] \right\} \times \mathbf{S}_1, \quad (8)$$

$$\dot{\mathbf{S}}_2 = \frac{(M\omega)^2}{2M} \left\{ \eta (M\omega)^{-1/3} \left(4 + 3 \frac{m_1}{m_2} \right) \hat{\mathbf{L}}_N + \frac{1}{M^2} \left[\mathbf{S}_1 - 3(\mathbf{S}_1 \cdot \hat{\mathbf{L}}_N) \hat{\mathbf{L}}_N \right] \right\} \times \mathbf{S}_2, \quad (9)$$

and the precession equation for $\hat{\mathbf{L}}_N$ is [10,18]

$$\dot{\hat{\mathbf{L}}}_N = \frac{\omega^2}{2M} \left\{ \left[\left(4 + 3 \frac{m_2}{m_1} \right) \mathbf{S}_1 + \left(4 + 3 \frac{m_1}{m_2} \right) \mathbf{S}_2 \right] \times \hat{\mathbf{L}}_N - \frac{3\omega^{1/3}}{\eta M^{5/3}} \left[(\mathbf{S}_2 \cdot \hat{\mathbf{L}}_N) \mathbf{S}_1 + (\mathbf{S}_1 \cdot \hat{\mathbf{L}}_N) \mathbf{S}_2 \right] \times \hat{\mathbf{L}}_N \right\}. \quad (10)$$

We stop the adiabatic evolution when the binary reaches the minimum energy circular orbit (MECO) defined by Eqs. (11)–(13) of Ref. [25]. The leading-order mass-quadrupole gravitational waveform can be obtained from Eqs. (65)–(78) of Ref. [25]. Those equations for the gravitational waveform, together with Eqs. (1)–(10), define our target model for precessing double-spin binaries.

Using the language of Ref. [25], precessing binaries of spinning BHs are described by the four *basic* (intrinsic) parameters m_1 , m_2 , $\mathbf{S}_1 \equiv |\mathbf{S}_1|$, $\mathbf{S}_2 \equiv |\mathbf{S}_2|$, by three *local* (intrinsic) parameters describing the relative orientation of the spins with respect to the angular momentum at a fiducial frequency (see Table I and Fig. 4 of Ref. [25]), and by five *directional* (extrinsic) parameters describing the relative orientation of the binary and the detector (see Table I of Ref. [25]). The waveforms depend also (if trivially) on two other extrinsic parameters, the initial phase Φ_0 and the time of arrival t_0 ; depending on the context, we shall at times omit these when counting the number of extrinsic parameters.

B. Search template family: single-spin binaries

As discussed in Sec. I, the results of previous investigations [18, 35, 25, 26] suggest that the gravitational waveforms emitted by double-spin binaries with comparable component masses can be approximated (at least for the purpose of detection with ground-based interferometers) by waveforms computed by neglecting spin-spin effects, and by assigning the total spin of the binary to a single BH. Thus, in this paper we examine the detection performance of the single-spin search family obtained from Eqs. (1)–(10) by setting $\mathbf{S}_2 = 0$. The simplified equations are

$$\frac{\dot{\omega}}{\omega^2} = \frac{96}{5} \eta_s (M_s \omega)^{5/3} \left[1 + \text{PN corrections} \right. \quad (11)$$

$$\left. - \frac{1}{12} (\hat{\mathbf{L}}_N \cdot \hat{\mathbf{S}}_{1s}) \chi_{1s} \left(113 \frac{m_{1s}^2}{M_s^2} + 75 \eta_s \right) (M_s \omega) \right],$$

$$\dot{\mathbf{S}}_{1s} = \frac{\eta_s (M_s \omega)^{5/3}}{2M_s} \left(4 + 3 \frac{m_{2s}}{m_{1s}} \right) \hat{\mathbf{L}}_N \times \mathbf{S}_{1s}, \quad (12)$$

$$\dot{\hat{\mathbf{L}}}_N = \frac{\omega^2}{2M_s} \left(4 + 3 \frac{m_{2s}}{m_{1s}} \right) \mathbf{S}_{1s} \times \hat{\mathbf{L}}_N, \quad (13)$$

where $M_s = m_{1s} + m_{2s}$, $\eta_s = m_{1s} m_{2s} / M_s^2$ and $\mathbf{S}_{1s} = \chi_{1s} m_{1s}^2 \hat{\mathbf{S}}_{1s}$. The “ s ” subscript stands for *search* parameters. In Eq. (11), “PN corrections” denotes the terms in Eqs. (2)–(7) that do not depend on the spins. The leading-order mass-quadrupole gravitational waveform is

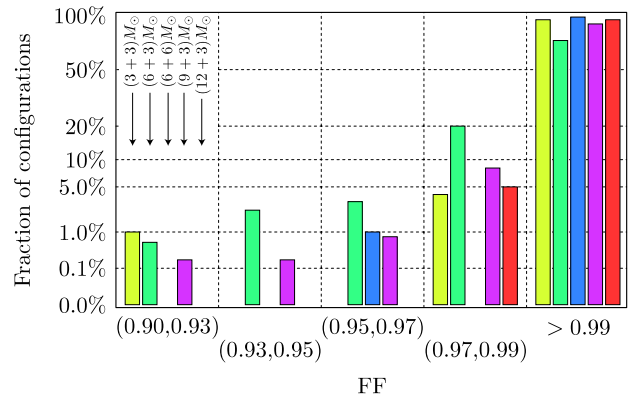


FIG. 1: Distribution of FFs for lower-mass ($M \leq 15M_\odot$) binary configurations. See the caption to Table I for an explanation of how the FF distributions were obtained.

given by Eqs. (65)–(78) and (11)–(13) of Ref. [25], after setting the spin of the lighter body to zero. This completes the definition of our single-spin search template family, which is parametrized by the four intrinsic parameters M_s , η_s , χ_{1s} , and $\kappa_{1s} = \hat{\mathbf{S}}_{1s} \cdot \hat{\mathbf{L}}_N$, and by five extrinsic parameters that describe the relative orientation of the detector and the binary (see Sec. III C of Ref. [26]). The maximization of the overlap with respect to the extrinsic parameters can be performed semi-algebraically, in two steps, as described in Sec. IV of Ref. [26].

We note that the simplified Eqs. (11)–(13) are exactly equivalent to the full Eqs. (1)–(10) in the two limits mentioned in Sec. I: for equal masses, if spin-spin effects are neglected; and for $m_1 \gg m_2$ (i.e., small η). To test the effectualness of the single-spin search templates in matching our target signals for binary configurations with both comparable and unequal masses, we computed the FF (i.e., the match, maximized over the intrinsic and extrinsic search parameters; see Sec. II) for target binaries with two maximal spins, and with masses $(m_1 + m_2) = (3+3)M_\odot$, $(6+3)M_\odot$, $(6+6)M_\odot$, $(9+3)M_\odot$, $(12+3)M_\odot$, $(10+10)M_\odot$, $(15+10)M_\odot$, and $(15+15)M_\odot$. In the $(12+3)M_\odot$ case we also considered a target binary with $\chi_1 = 1/16$ and $\chi_2 = 1$, i.e. the two objects possess equal magnitude of spins, while the less massive one is maximally spinning. Search and target signals were always obtained at 2PN order, and the computation of the FF was repeated for 100 or 500 (for the lighter binaries) randomly generated configurations of the target-signal local parameters $\hat{\mathbf{L}}_N$, $\hat{\mathbf{S}}_1$ and $\hat{\mathbf{S}}_2$, assuming uniform and independent angular distributions. The directional parameters of the target signals were fixed to arbitrary values without loss of generality, since for the purpose of

templates:	$(3+3)M_\odot$		$(6+3)M_\odot$		$(6+6)M_\odot$		$(9+3)M_\odot$		$(12+3)M_\odot$	
	with spin	nospin	with spin	with spin	no spin	with spin	with spin	with spin	equal-spin target	
$\text{FF} \geq 0.99$	95%	31%	74%	98%	59%	90%	95%	84%		
$\text{FF} < 0.99$	5%	69%	26%	2%	41%	10%	5%	16%		
$\text{FF} < 0.95$	0%	38%	3%	0%	25%	1%	0%	0%		
lowest FF	0.9085	0.7042	0.9119	0.7250	0.6391	0.8945	0.9734	0.9684		
$\overline{\text{FF}}$	≥ 0.989	≥ 0.938	≥ 0.986	≥ 0.987	≥ 0.934	≥ 0.989	≥ 0.990	≥ 0.990		

templates:	$(10+10)M_\odot$		$(15+10)M_\odot$		$(15+15)M_\odot$	
	with spin	nospin	with spin	no spin	with spin	no spin
$\text{FF} \geq 0.99$	100%	29%	98%	22%	100%	30%
$\text{FF} < 0.99$	0%	71%	2%	78%	0%	70%
$\text{FF} < 0.95$	0%	34%	0%	46%	0%	31%
lowest FF	0.9754	0.7142	0.9691	0.7138	≥ 0.99	0.7546
$\overline{\text{FF}}$	≥ 0.990	≥ 0.945	≥ 0.990	≥ 0.936	≥ 0.990	≥ 0.957

TABLE I: Summary of FFs between the single-spin search template family and the double-spin target model. The numerical maximization procedure is stopped whenever a $\text{FF} \geq 0.99$ is achieved. The upper table shows results for lower-mass binaries ($M \leq 15M_\odot$); the lower table for higher-mass binaries ($M \geq 20M_\odot$). In the first three rows of each table, we list the percentage of systems yielding FFs ≥ 0.99 , < 0.99 and < 0.95 , in a population of 100 target systems [500 for $(m_1 + m_2) = (6+3)M_\odot$ and $(9+3)M_\odot$ binaries] with maximal spins and random, uniform distributions of initial spin and detector orientations (local parameters). In the fourth row we list the lowest FFs found among the population; in the last row, we list the average FFs [when a $\text{FF} \geq 0.99$, we use 0.99 in computing the average.] The distribution of the FFs for selected mass configurations is also histogrammed in Fig. 1. The target and search waveforms are computed by starting the integration of the equations of motion at an instantaneous GW frequency of 60 Hz and 40 Hz for upper and lower tables, respectively. For some mass configurations we show also the FFs for nonspinning templates (i.e., single-spin templates where χ_{1s} was set to zero), and for $(12+3)M_\odot$ binaries, we show the FFs for a target configuration with $\chi_1 = 1/16$ and $\chi_2 = 1$ (i.e., the S_2 is maximal and $S_1 = S_2$).

computing FFs they are degenerate with respect to the local parameters (see Sec. VI A of Ref. [25]).

The results of our tests are listed in Table I, and plotted in Fig. 1. For comparison, in Table I we include also some FFs computed for the nonspinning search templates obtained by setting χ_{1s} to zero in Eqs. (11)–(13). Our numbers support our conjecture about the effectuality of the single-spin search family. More specifically:

- Spin-spin effects are not important for higher-mass binaries such as $(15+15)M_\odot$, $(15+10)M_\odot$ and $(10+10)M_\odot$, where FFs are consistently very high; however, spin-orbit effects cannot be neglected, as shown by the relatively low FFs achieved by the nonspinning search family.
- For lower-mass binaries such as $(3+3)M_\odot$ and $(6+6)M_\odot$, FFs are also very high, with few exceptions: thus, although in these binaries spin-spin effects can accumulate over many GW cycles within the band of good detector sensitivity, they rarely become comparable to spin-orbit effects.
- For low-mass-ratio binaries such as $(12+3)M_\odot$ ($\eta = 0.16$), FFs are high, since the spin of the heavier object dominates the precessional dynamics. If we reduce the magnitude of S_1 so that $S_1 = S_2$, the resulting FFs become lower, because the dynamics deviates farther from both the single-spin

and equal-mass limits.

- The worst FFs are obtained for $(6+3)M_\odot$ and $(9+3)M_\odot$ binaries, which have rather low total masses, and intermediate mass ratios (thus, they sit halfway between the two single-spin equivalence limits). In this case, double-spin effects cannot be reproduced with accuracy by single-spin systems (in Sec. III D we shall examine in more detail what is happening there). Note however that this happens only for a limited number of angular configurations, so the average of the FF over the sampling is still very high.

The range of search-template parameters needed to yield the high FFs discussed above extends beyond values that would be physical for a real single-spin binary, with $\eta_s > 0.25$ and $\chi_{1s} > 1$. This is to be expected: consider, for instance, that in the equal-mass case the equivalence between the simplified and the full equations implies values of χ_{1s} up to 2. In Fig. 2 we show the parameters of the best-fit search templates corresponding to target signals with the test masses examined above [augmented by $(15+3)M_\odot$, $(12+6)M_\odot$, and $(15+12)M_\odot$]. As shown in the top panel, the search-template images of target signals with the same masses but different local parameters are spread around the nominal (M_s, η_s) values (indicated by the end of the thin lines, and always enclosed within

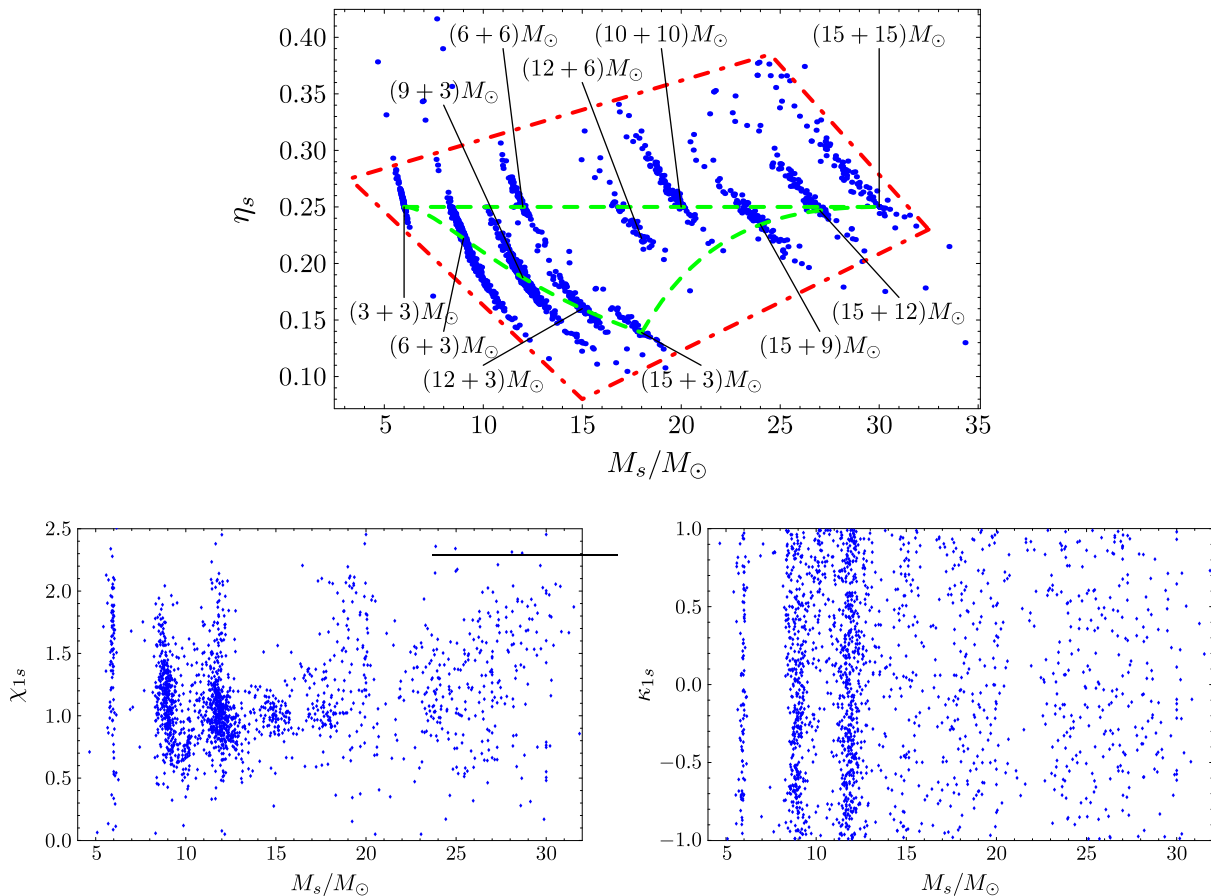


FIG. 2: Location in the (intrinsic) search parameter space $(M_s, \eta_s, \chi_{1s}, \kappa_{1s})$ of the best-fit templates for target signals with $(m_1 + m_2) = (3 + 3)M_\odot, (6 + 3)M_\odot, (9 + 3)M_\odot, (12 + 3)M_\odot, (15 + 3)M_\odot, (6 + 6)M_\odot, (12 + 6)M_\odot, (10 + 10)M_\odot, (15 + 10)M_\odot, (15 + 12)M_\odot,$ and $(15 + 15)M_\odot$, with maximal spins, and with random angular distributions of the initial $\hat{\mathbf{L}}_N, \mathbf{S}_1, \mathbf{S}_2$. Dots are denser for the $(6 + 3)M_\odot$ and $(9 + 3)M_\odot$ configurations, for which more FF were computed. In the (M_s, η_s) scatter plot (on top), the dashed contour encloses the region obtained by setting $M_s = M$ and $\eta_s = \eta$, and by taking $(m_1, m_2) \in [3, 15]M_\odot \times [3, 15]M_\odot$. The dotted and dashed line, drawn somewhat arbitrarily, encloses a possible template bank boundary, used in Sec. IV to estimate the number of templates necessary to search for double-spin binaries in this mass range. The labels identify the search template clusters corresponding to each target mass configuration, and they are connected to the nominal projection point obtained by setting $M_s = M$ and $\eta_s = \eta$.

the dashed contour). The uncertainty in target parameter estimation induced by this spreading is discussed in Sec. V. In the same panel, the dotted-dashed line encloses the template-bank boundary used in Sec. IV to estimate the number of templates necessary for a search of systems with masses $(m_1, m_2) \in [3, 15]M_\odot \times [3, 15]M_\odot$. The bottom panels show the range achieved by the search parameters χ_{1s} and κ_{1s} , which is comparable to the range of the analogous target parameters, $|\mathbf{S}_{\text{tot}}|/m_1^2$ and $\kappa_{\text{tot}} \equiv \hat{\mathbf{S}}_{\text{tot}} \cdot \hat{\mathbf{L}}_N$.

C. On the robustness of waveforms across PN orders

In the previous section we have established that single-spin waveforms are good approximations for double-spin

waveforms, at least within the mass range under consideration. However, whether double-spin waveforms are representative of actual physical signals is an entirely different question, which hinges on the validity of the circular adiabatic approximation, but also on the robustness of the waveforms under change of PN order: if the waveforms change substantially with increasing order, we should suspect that the description of the physics is incomplete without higher-order terms yet to be computed.

Studying the robustness of double-spin binaries is technically difficult, since it means computing the FF between two template families (of different PN order) with seven intrinsic parameters. This entails the delicate numerical maximization of a seven-parameter function whose evaluation is relatively costly. Instead, we choose to perform our study on single-spin waveforms, and then argue that the results should transfer to double-spin

$(N+k, N)$	$\langle \text{ST}_{N+k}, \text{ST}_N \rangle$ for $(10+10)M_\odot$ binary, $M = 20M_\odot$, $\eta = 0.250$			
	$\kappa_1 = 0.9$	$\kappa_1 = 0.5$	$\kappa_1 = -0.5$	$\kappa_1 = -0.9$
(1,0)	0.3136 (0.6688) [16.1,0.25,0.00, 0.00]	0.3136 (0.6688)	0.3136 (0.6688) [16.1,0.25,0.00,-0.00]	0.3136 (0.6688)
(1.5,1)	0.3123 (0.5922) [23.7,0.25,0.00, 0.00]	0.2676 (0.5137)	0.2306 (0.4860) [29.2,0.25,0.00,-0.00]	0.2160 (0.4543)
(2,1.5)	0.7124 (0.9823) [19.2,0.25,1.00, 0.99]	0.7222 (0.9877)	0.8545 (0.9886) [19.3,0.25,1.00,-0.66]	0.8601 (≥ 0.99)
(2.5,2)	0.2851 (0.8702) [18.8,0.25,1.00, 0.91]	0.3099 (0.9206)	0.4166 (≥ 0.99) [20.4,0.25,1.00, 0.81]	0.4682 (≥ 0.99)
(3,2)	0.9604 (≥ 0.99) [20.2,0.25,0.88, 0.79]	0.9743 (≥ 0.99)	0.9915 (≥ 0.99) [19.7,0.24,0.88,-0.23]	0.9805 (≥ 0.99)
(3,2.5)	0.2848 (0.9846) [18.8,0.25,1.00,-0.31]	0.2898 (≥ 0.99)	0.4027 (0.9823) [20.4,0.25,1.00,-0.99]	0.4634 (0.9740)
(3.5,3)	0.9316 (≥ 0.99) [20.2,0.25,1.00, 0.90]	0.9475 (≥ 0.99)	0.9749 (≥ 0.99) [19.7,0.25,1.00,-0.99]	0.9744 (≥ 0.99)

$(N+k, N)$	$\langle \text{ST}_{N+k}, \text{ST}_N \rangle$ for $(15+10)M_\odot$ binary, $M = 25M_\odot$, $\eta = 0.247$			
	$\kappa_1 = 0.9$	$\kappa_1 = 0.5$	$\kappa_1 = -0.5$	$\kappa_1 = -0.9$
(1,0)	0.3124 (0.6030) [19.1,0.25,0.00,0.00]	0.3124 (0.6030)	0.3124 (0.6030) [19.1,0.25,0.00,-0.00]	0.3124 (0.6030)
(1.5,1)	0.2784 (0.4994) [31.0,0.25,0.00,0.00]	0.2732 (0.4684)	0.2466 (0.3913) [41.9,0.25,0.00,-0.00]	0.1896 (0.3491)
(2,1.5)	0.5810 (≥ 0.99) [24.8,0.23,1.00,0.98]	0.8038 (≥ 0.99)	0.8644 (≥ 0.99) [25.4,0.24,1.00,-0.59]	0.9067 (≥ 0.99)
(2.5,2)	0.2558 (0.8525) [22.9,0.23,1.00,0.95]	0.3296 (0.9280)	0.5022 (≥ 0.99) [25.5,0.24,1.00, 0.80]	0.5921 (≥ 0.99)
(3,2)	0.9106 (≥ 0.99) [24.8,0.24,0.88,0.73]	0.9392 (≥ 0.99)	0.9858 (≥ 0.99) [25.1,0.23,0.89,-0.21]	0.9650 (≥ 0.99)
(3,2.5)	0.2520 (0.9148) [27.0,0.25,1.00,0.85]	0.2942 (≥ 0.99)	0.4552 (≥ 0.99) [25.7,0.24,1.00,-0.59]	0.5333 (≥ 0.99)
(3.5,3)	0.9264 (≥ 0.99) [24.9,0.24,1.00,0.90]	0.9528 (≥ 0.99)	0.9769 (≥ 0.99) [25.3,0.24,1.00,-0.36]	0.9839 (≥ 0.99)

$(N+k, N)$	$\langle \text{ST}_{N+k}, \text{ST}_N \rangle$ for $(15+15)M_\odot$ binary, $M = 30M_\odot$, $\eta = 0.250$			
	$\kappa_1 = 0.9$	$\kappa_1 = 0.5$	$\kappa_1 = -0.5$	$\kappa_1 = -0.9$
(1,0)	0.2710 (0.5158) [22.5,0.25,0.00, 0.00]	0.2710 (0.5158)	0.2710 (0.5158) [22.5,0.25,0.00,-0.00]	0.2710 (0.5158)
(1.5,1)	0.2694 (0.4050) [38.3,0.25,0.00, 0.00]	0.2145 (0.3644)	0.2435 (0.3155) [49.6,0.25,0.00,-0.00]	0.1855 (0.2797)
(2,1.5)	0.7619 (≥ 0.99) [31.1,0.25,1.00, 0.89]	0.8613 (≥ 0.99)	0.9018 (≥ 0.99) [30.6,0.25,1.00,-0.43]	0.8946 (≥ 0.99)
(2.5,2)	0.3403 (0.9086) [28.0,0.24,0.92, 0.99]	0.3856 (0.9237)	0.5372 (≥ 0.99) [30.4,0.25,1.00, 0.95]	0.6216 (≥ 0.99)
(3,2)	0.9330 (≥ 0.99) [28.8,0.24,0.90, 0.82]	0.9360 (≥ 0.99)	0.9641 (≥ 0.99) [30.3,0.24,0.88, 0.17]	0.9612 (≥ 0.99)
(3,2.5)	0.2926 (≥ 0.99) [28.1,0.25,1.00,-0.58]	0.3549 (≥ 0.99)	0.4893 (≥ 0.99) [31.0,0.25,1.00,-0.67]	0.5498 (≥ 0.99)
(3.5,3)	0.9265 (≥ 0.99) [30.4,0.25,0.90, 0.71]	0.9456 (≥ 0.99)	0.9814 (≥ 0.99) [29.1,0.25,1.00,-0.30]	0.9831 (≥ 0.99)

TABLE II: Test of robustness of the PN adiabatic waveforms ST_N (defined in Sec. III A) across PN orders, for $(m_1 + m_2) = (10+10)M_\odot$, $(15+10)M_\odot$ and $(15+15)M_\odot$. We set $\chi_1 = 1$, $\chi_2 = 0$, and $\kappa_1 = -0.9, -0.5, 0.5$, and 0.9 . The matches quoted at the beginning of each column are maximized only with respect to the extrinsic parameters t_0 and Φ_0 . In parentheses, “(...)”, we give the matches maximized over all the parameters of the lower-order family (i.e., the fitting factors FF for the target family ST_{N+k} as matched by the search family ST_N , evaluated at the ST_{N+k} intrinsic parameters indicated). In brackets, “[...]”, we give the parameters M , η , χ_1 , and κ_1 (or M and η at 1PN and 1.5PN orders when spin terms are absent) at which the FF is achieved. The detector is set perpendicular to the initial orbital plane, and at 3PN and 3.5PN order we set $\hat{\theta} = 0$; in all cases the integration of the equations of motion starts at an instantaneous GW frequency of 40 Hz. [See Refs. [17, 25] for a discussion of why for some mass combinations the 2.5PN model differs so much from the other orders.]

waveforms because the search and target families are close. Thus, our study is very similar to the Cauchy convergence test of Ref. [26], except for the choice of masses: here we focus on binaries at the higher-mass end of our range, since these systems are expected to have stronger higher-order PN effects within the frequency band of good interferometer sensitivity.

For $(m_1 + m_2) = (10+10)M_\odot$, $(15+10)M_\odot$, and $(15+15)M_\odot$, we list in Table II the matches across PN orders, maximized only on t_0 and Φ_0 ; the numbers in parentheses, “(...)”, give the FF for the higher-order family as matched by the lower-order family, and the numbers in brackets, “[...]”, give the intrinsic parameters where the FF is attained. The tests are performed for $\chi_{1s} = 1$, for

different values of κ_{1s} , and for a GW detector in a direction (with respect to the binary) perpendicular to normal vector of the initial orbital plane, which should be representative of the generic effects of precession. The high FFs obtained between the 2PN and the higher-order families suggest that the 2PN model is already representative of the variety of waveforms expected from actual sources; on the other hand, the lower direct matches (and the biased values of search parameters at the FF) suggest that the family of the highest available order should be used for source parameter estimation. It would be worthwhile to evaluate the FF between the double-spin (and indeed, single-spin) adiabatic model, and nonadiabatic models based on resummed PN equations [16, 17, 36, 37], espe-

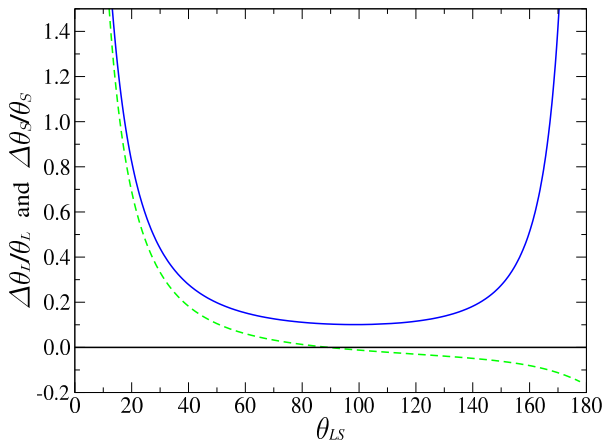


FIG. 3: Relative change of the opening angles as function of θ_{LS} for a $(6+3)M_\odot$ binary, with $\chi_{\text{tot}} = 0.4$, $|\mathbf{L}| = |\mathbf{L}_N| = \eta M^{5/3} \omega^{-1/3}$, and $\omega = 2\pi \times 30$ Hz. The change shown corresponds to a 10% increase in $|\mathbf{S}_{\text{tot}}|$. The solid and dashed curves refer to θ_L and θ_S , respectively.

cially when these predict the end of the inspirals within the band of good interferometer sensitivity.

D. Some features of the dynamics of double-spin binaries

In this section we study the precessional dynamics of double-spin binaries, with the purpose of building a physical understanding of the matching performance of single-spin templates observed in Sec. III B; in particular, we wish to identify what features of double-spin dynamics, absent in single-spin systems, lead to the low FFs seen for lower-mass binary configurations.

From Eqs. (8)–(10), we see that the precession of double-spin binaries preserves both $\hat{\mathbf{J}}$ and $|\mathbf{L}|$ at timescales shorter than the radiation-reaction timescale—at which $|\mathbf{L}|$ decreases steadily. Even at longer timescales, as recognized by ACST for single-spin binaries and further tested by BCV2 for generic double-spin binaries, for the vast majority of configurations the

direction of the total angular momentum remains almost constant ($\dot{\hat{\mathbf{J}}} \simeq 0$); this behavior is known as *simple precession*.

For single-spin binaries, or for equal-mass binaries if we ignore the spin-spin interaction, the angle between \mathbf{L} and \mathbf{S}_{tot} (θ_{LS}) remains fixed all through evolution [according to Eqs. (8)–(10)]; for simple precession, this implies that the angle between \mathbf{L} and $\hat{\mathbf{J}}$ (θ_L) must increase, and that the angle between \mathbf{S}_{tot} and $\hat{\mathbf{J}}$ (θ_S) must decrease—both do so monotonically, at the radiation-reaction timescale. In summary, in these binaries the orbital plane precesses while its inclination increases slowly and monotonically.

In Ref. [21], Apostolatos investigated the effect of spin-spin coupling on the dynamical evolution of *equal-mass, equal-spin* BH–BH binaries. He obtained analytical solutions for the opening-angle products $\hat{\mathbf{S}}_{1,2} \cdot \hat{\mathbf{J}}$ and $\hat{\mathbf{S}}_1 \cdot \hat{\mathbf{S}}_2$ to first order in S/L , where J is the total angular momentum, S is S_1 or S_2 , and L is the orbital angular momentum (if $m_1 \sim m_2$, then throughout all the inspiral $S \ll L$ [18]). The main feature identified by Apostolatos was that the orbital plane not only becomes slowly more inclined (at the radiation-reaction timescale), but the spin-spin interaction also causes a *nutation*; namely, an oscillation of the orbital inclination angle (θ_L) at the timescale of the spin-spin interaction.

In the following, we shall relax the assumption that the BH masses are equal, and we shall investigate what the consequences are on the evolution of $\hat{\mathbf{S}}_{1,2} \cdot \hat{\mathbf{J}}$ and $\hat{\mathbf{S}}_1 \cdot \hat{\mathbf{S}}_2$. To simplify our notation we fix $m_1 + m_2 = 1$, and we introduce the parameter $\delta \equiv m_1 - m_2$, which describes the deviation from the equal-mass case. We keep only terms up to linear order in δ . We then have (assuming as always $m_1 \geq m_2$)

$$m_1 = \frac{1+\delta}{2}, \quad m_2 = \frac{1-\delta}{2}, \quad (14)$$

$$S_1 = m_1^2 \chi_1 \simeq \frac{1}{4} (1+2\delta) \chi_1, \quad (15)$$

$$S_2 = m_2^2 \chi_2 \simeq \frac{1}{4} (1-2\delta) \chi_2. \quad (16)$$

Inserting these definitions into Eqs. (8) and (9) leads to

$$\frac{d}{dt}(\hat{\mathbf{S}}_1 \cdot \hat{\mathbf{J}}) = \frac{\omega^2}{2} S_2 \left[\overbrace{(7-6\delta)}^{\text{spin-orbit}} - \overbrace{\left(1 + 3 \frac{\mathbf{J} \cdot \mathbf{S}_2}{L^2}\right)}^{\text{spin-spin}} \right] \hat{\mathbf{J}} \cdot (\hat{\mathbf{S}}_1 \times \hat{\mathbf{S}}_2), \quad (17)$$

$$\frac{d}{dt}(\hat{\mathbf{S}}_2 \cdot \hat{\mathbf{J}}) = \frac{\omega^2}{2} S_1 \left[\overbrace{(7+6\delta)}^{\text{spin-orbit}} - \overbrace{\left(1 + 3 \frac{\mathbf{J} \cdot \mathbf{S}_1}{L^2}\right)}^{\text{spin-spin}} \right] \hat{\mathbf{J}} \cdot (\hat{\mathbf{S}}_2 \times \hat{\mathbf{S}}_1), \quad (18)$$

$$\frac{d}{dt}(\hat{\mathbf{S}}_1 \cdot \hat{\mathbf{S}}_2) = \frac{\omega^2}{2} \left[\overbrace{(-12\delta)}^{\text{spin-orbit}} + \overbrace{\left(3 \frac{\mathbf{J} \cdot (\mathbf{S}_1 - \mathbf{S}_2)}{L^2}\right)}^{\text{spin-spin}} \right] \hat{\mathbf{J}} \cdot (\hat{\mathbf{S}}_1 \times \hat{\mathbf{S}}_2). \quad (19)$$

Following Apostolatos, in deriving these equations we have assumed that $S \ll L$, $L = J [1 + \mathcal{O}(S/L)]$, and that the direction of the total angular momentum remains almost constant during evolution. In Eqs. (17)–(19) we have separated the terms due to spin-orbit and spin-spin interactions.

According to Eq. (19), in the equal-mass case ($\delta = 0$) without spin-spin effects, the angle between $\hat{\mathbf{S}}_1$ and $\hat{\mathbf{S}}_2$ is constant; generically, however, the spin-spin and even the spin-orbit interactions can cause that angle (and hence the magnitude of \mathbf{S}_{tot}) to change. As first observed by ACST and further investigated by Apostolatos [21], this variation in $|\mathbf{S}_{\text{tot}}|$ drives the nutation of the orbital plane: oscillations are superimposed to the monotonic evolution of the angles between $\hat{\mathbf{L}}$ and $\hat{\mathbf{J}}$ (θ_L) and between $\hat{\mathbf{S}}_{\text{tot}}$ and $\hat{\mathbf{J}}$ (θ_S) [21], as can be understood from the following simple argument. Recall that on timescales shorter than the radiation-reaction timescale, $|\mathbf{L}|$ and \mathbf{J} are conserved; using δ to denote the change in the dynamical variables incurred during such a time, we write

$$\delta|\mathbf{J}|^2 = 0, \quad \delta|\mathbf{L}|^2 = 0 \quad (20)$$

to get

$$2\delta(\mathbf{L} \cdot \mathbf{S}_{\text{tot}}) = -\delta(|\mathbf{S}_{\text{tot}}|^2). \quad (21)$$

Using $\delta\mathbf{J} = 0$ we then have

$$\delta\lambda_L = -\frac{1}{2LJ}\delta(|\mathbf{S}_{\text{tot}}|^2) \quad \text{for} \quad \lambda_L = \frac{\mathbf{L} \cdot \mathbf{J}}{LJ}, \quad (22)$$

and

$$\delta\lambda_S = -\frac{\mathbf{L} \cdot \mathbf{S}_{\text{tot}}}{2S_{\text{tot}}^3 J}\delta(|\mathbf{S}_{\text{tot}}|^2) \quad \text{for} \quad \lambda_S = \frac{\mathbf{S}_{\text{tot}} \cdot \mathbf{J}}{S_{\text{tot}} J}. \quad (23)$$

Thus, when $|\mathbf{S}_{\text{tot}}|$ oscillates, the opening angles θ_L and θ_S oscillate as well; in fact, we have

$$\delta\theta_L = \frac{1}{2|\mathbf{L} \times \mathbf{S}_{\text{tot}}|}\delta(|\mathbf{S}_{\text{tot}}|^2), \quad (24)$$

$$\delta\theta_S = \frac{\mathbf{L} \cdot \mathbf{S}_{\text{tot}}}{2|\mathbf{S}_{\text{tot}}|^2|\mathbf{L} \times \mathbf{S}_{\text{tot}}|}\delta(|\mathbf{S}_{\text{tot}}|^2), \quad (25)$$

which suggests that, for the same variation in $|\mathbf{S}_{\text{tot}}|^2$, the nutation is most significant when \mathbf{L} and \mathbf{S} are either nearly aligned or antialigned. In Fig. 3, we plot the relative changes in θ_L and θ_S as functions of the angle between \mathbf{L} and \mathbf{S} ($\theta_{LS} = \theta_L + \theta_S$), choosing a fixed positive $\delta(|\mathbf{S}_{\text{tot}}|)$. The change is always positive for θ_L , while it can be negative for θ_S , if $\theta_{LS} > 90^\circ$. In addition, the relative changes *diverge* near $\theta_{LS} \sim 0^\circ$ or 180° . These features follow straightforwardly from Eqs. (24) and (25).

Spin-spin effects. When spin-spin effects are included, the angle between $\hat{\mathbf{S}}_1$ and $\hat{\mathbf{S}}_2$ oscillates according to the second term on the right-hand side of Eq. (19). However, as evidenced by the FF results for equal-mass binaries given in Sec. III B, the amplitude of these oscillations does not seem to be very large, and the nutation

of the orbital plane does not complicate significantly the waveforms, at least as evaluated at the leading mass-quadrupole order.

Spin-orbit effects. From the first term on the right-hand side of Eq. (19), we see that even in the absence of spin-spin effects, unequal masses (i.e., $\delta \neq 0$) can cause the evolution of $\hat{\mathbf{S}}_1 \cdot \hat{\mathbf{S}}_2$, and therefore drive the nutation of the orbital plane. Spin-orbit effects, which come in at a lower PN order, can sometimes be more significant than spin-spin effects, especially for binaries with intermediate mass ratios, such as $(m_1 + m_2) = (6+3)M_\odot$ and $(9+3)M_\odot$ binaries; indeed, these effects could explain the lower FFs found in Sec. III B for those systems.

Examples of combined spin-spin and spin-orbit effects in double-spin binaries leading to oscillations in $|\mathbf{S}_{\text{tot}}|$, and therefore θ_L and θ_S , are shown in Fig. 4 for systems with $(m_1 + m_2) = (6 + 3)M_\odot$ ($\delta = 1/3$), and with initial local parameters such that $\text{FF} \geq 0.99$ (on the left) and $\text{FF} \sim 0.94$ (on the right). The nutation behavior evident in these figures is well described by the approximated equations (24) and (25). For comparison we show (as continuous lines) also the evolution of the analogous quantities in the best-fit single-spin configurations; for these, the opening angles θ_L and θ_S evolve monotonically. Lower overlaps seem to correspond to initial conditions for which nutation is rather significant and overwhelms the underlying monotonic evolution. In Fig. 5 we show the percentage of configurations with $\text{FF} \leq 0.99$ (light pattern) and $\text{FF} \leq 0.97$ (dark pattern) as a function of the initial $\lambda_{LS} \equiv \hat{\mathbf{L}}_N \cdot \hat{\mathbf{S}}_{\text{tot}}$ (evaluated at the starting frequency [38]), for $(6 + 3)M_\odot$ and $(9 + 3)M_\odot$ binaries. The plot suggests that lower FFs are more likely to occur when the initial $\hat{\mathbf{L}} \cdot \hat{\mathbf{S}}_{\text{tot}} \simeq \pm 1$, which is consistent with the fact that nutation is most significant when $\theta_{LS} \sim 0^\circ$ or 180° [39].

Figure 5 shows also an asymmetry in the distribution of low FFs, which are denser when $\theta_{LS} < 90^\circ$. Currently we do not have a clear understanding of this behaviour [40]. It is worth pointing out that this asymmetry and, more in general, the low FFs observed could be due to other features of double-spin dynamics that cannot be reproduced by single-spin systems, but that are difficult to dig out by analysis or numerical experiment, in the absence of a full analytical solution to the precession equations. Moreover, some of the low FFs might be due to shortcomings in our numerical optimization procedure in cases where the match surface in the search parameter space has an especially convoluted geometry.

IV. TEMPLATE SPACE AND NUMBER OF TEMPLATES

In this section we estimate the number of single-spin templates necessary to search for double-spin signals with single masses in the $[3, 15]M_\odot$ range. To do this, we compute the average projected metric $\overline{g_{ij}^{\text{proj}}}$ in the (M_s, η_s) region delimited by the dashed and dotted contour of

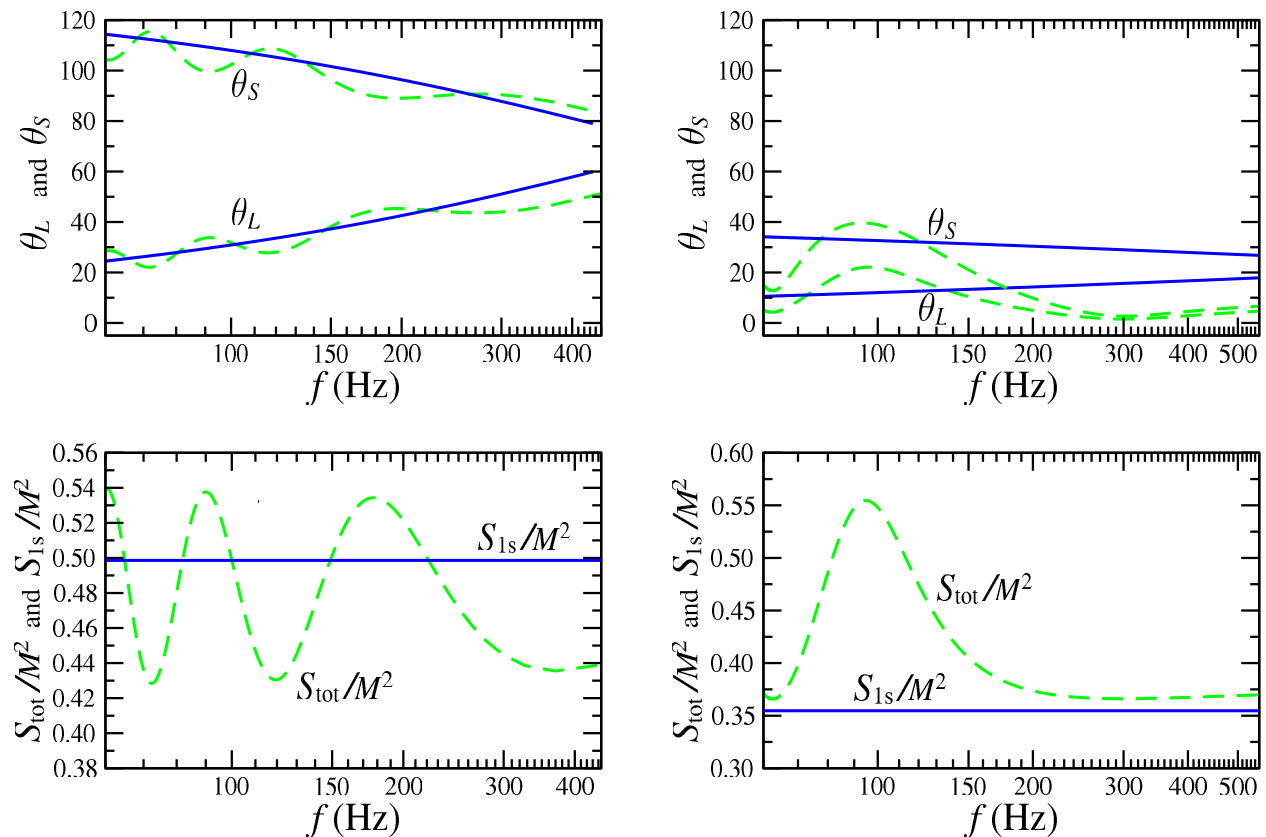


FIG. 4: Evolution of the opening angles θ_L and θ_S , and of the total-spin magnitude S_{tot} (all plotted as dashed lines) for double-spin target systems yielding $\text{FF} \geq 0.99$ (left column) and $\text{FF} \simeq 0.94$ (right column) when matched by single-spin templates; the target system has $(m_1 + m_2) = (6 + 3)M_\odot$. For comparison, the solid lines show the evolution of the analogous single-spin quantities [θ_L , $\theta_S = \arccos(\hat{\mathbf{S}}_{1s} \cdot \hat{\mathbf{J}})$, and S_{1s}] for the best-fit single-spin systems.

Fig. 2, following the procedure described in Sec. VI of Ref. [26]. We notice the presence of reduction curves connecting (roughly) the segment $\chi_{1s} \in [0, 2]$, $\kappa_{1s} = 0$ to the entire (χ_{1s}, κ_{1s}) plane in the search template space. Thus, we select a 3-D reduced template space corresponding to (M_s, η_s) within the quadrilateral with vertexes $(15M_\odot, 0.08)$, $(3.25M_\odot, 0.275)$, $(32.5M_\odot, 0.23)$, $(24.5M_\odot, 0.385)$, to $\chi_{1s} \in [0, 2]$, and to $\kappa_{1s} = 0$. Additional subfamilies might be needed to deal with certain singularities that we observe in the reduction curves as κ_{1s} gets close to ± 1 , but our selection should already give us an acceptable idea of the number of necessary templates, which is computed according to

$$\mathcal{N}_{\text{templates}} = \frac{\int \sqrt{|\det g_{i'j'}^{\text{proj}}|} dM_s d\eta_s d\chi_{1s}}{\left[2\sqrt{(1 - \text{MM})/3}\right]^3}, \quad (26)$$

where the primed indices i', j' run through M_s, η_s , and χ_{1s} ; the metric is averaged over 1,000 sets of target extrinsic parameters. The integral is carried out by evaluating the projected metric (a computationally expensive operation) at 80 points within the integration region, and

filling it by *natural neighbor interpolation* [41]. The final result is $\mathcal{N}_{\text{templates}} \simeq 320,000$ for $\text{MM} = 0.98$ (not including a reduction mismatch of ~ 0.01 incurred along the reduction curves [26]). Given the uncertainties implicit in the numerical computation of the metric, in the interpolation, in the choice of the reduction curves, and in the actual placement of the templates in the bank, this number should be understood only as an order-of-magnitude estimate. Most of the templates, by a factor of many, come from the lower part of the integration region (i.e., from the lowest η_s for any given M_s); about 100,000 out of 320,000 come from the region with $\chi_{1s} < 1$.

V. ESTIMATION OF BINARY PARAMETERS

Since the single-spin template family contains only a subset (of lower dimensionality) of all possible double-spin waveforms, we cannot expect to obtain estimates of all the physical parameters of double-spin systems from a single-spin-template search. The most straightforward way to recover those parameters would be to perform a search using double-spin templates after single-spin tem-

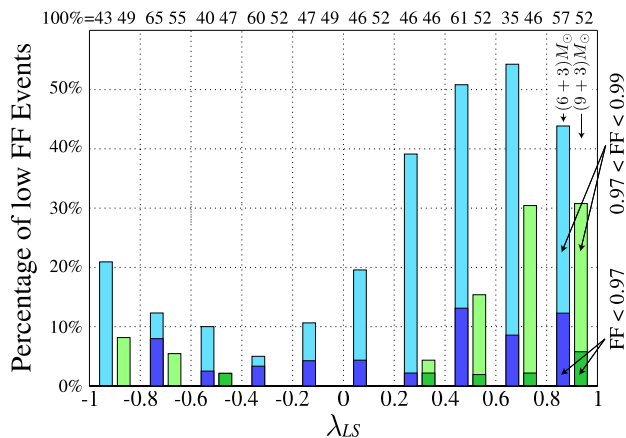


FIG. 5: Percentage of initial spin configurations that yield $\text{FF} \leq 0.99$ (light pattern) and $\text{FF} \leq 0.97$ (dark pattern), as a function of the initial opening angle product $\lambda_{LS} = \hat{\mathbf{L}} \cdot \hat{\mathbf{S}}_{\text{tot}}$, for $(m_1 + m_2) = (6+3)M_{\odot}$ and $(9+3)M_{\odot}$ binaries. The numbers on top show the total number of configurations (among 500) randomly extracted within each bin of $\Delta\lambda_{LS} = 0.2$.

plates have yielded a detection; such a follow-on search may be computationally feasible, since double-spin templates will then be applied only to the data stretches that have been established to contain signals. However, it is still meaningful to analyze the parameter-estimation performance of the single-spin template family, since any constraints on source parameters will decrease the size of the double-spin template bank necessary for the follow-on search, lowering the computational cost even further. In addition, this analysis can offer further useful insight into the FF map of double-spin into single-spin waveforms.

Double-spin target waveforms are parametrized by twelve parameters (seven intrinsic, and five extrinsic), while single-spin search templates are parametrized by nine (four intrinsic, M_s , η_s , χ_{1s} , and κ_{1s} ; and five extrinsic). Thus, maximizing the match over the search parameters induces a map from the 12-parameter target-signal space into the 9-parameter template space. The inverse map takes each point in the template space into a 3-dimensional manifold in the target-signal space, whose size indicates the extent to which the physical parameters of the double-spin binary can be constrained. Unfortunately, evaluating the size of the inverse image requires computational resources well beyond what is currently available to us. Furthermore, such a procedure can only be meaningful after *statistical error* has also been taken into account: because the detector output contains also noise, the template parameters at which we obtain the maximal correlation between template and data (the *actual* projection point) will differ, by a random statistical error, from the parameters at which the correlation between template and *signal* is highest (the *theoretical* projection point) [42]. We leave the quantitative study of statistical errors to a forthcoming paper [43].

In this paper we take a semi-quantitative approach.

We ignore the extrinsic parameters, so we study the map of seven parameters into four; then, we identify a number of intrinsic parameters of the double-spin binary (our *target observables*), and we explore how well we can estimate their values using functions of the four intrinsic parameters of the best-fit single-spin template (our *estimators*). We use three general criteria in the choice of target observables and estimators:

Consistency. The target observables and estimators should coincide when the double-spin system is dynamically equivalent to a single-spin system (according to the criteria spelled out in Sec. I).

Robustness. The definitions of the target observables and of the estimators should be independent of the detector noise curve; equivalently, the target observables should be (almost) conserved quantities (we already know that the four template parameters, and hence the estimators, are conserved).

Strong influence. The target observables, and therefore the estimators, should have a strong influence to the waveforms. Quantitatively, we can require the mismatch metric to have large components along the direction of change of the target observables and estimators; it follows that the target observables and estimators should remain essentially constant along eventual reduction curves.

This criterion is important for two reasons: first, the 7-to-4-dimensional FF map is unlikely to preserve unessential features of the target space; second, even if the map preserved these features, statistical error would inevitably spoil their estimation, because the associated mismatch-metric components are small. A third reason, contingent on our implementation of the FF search, is that we stop the maximization of the match whenever this reaches 0.99; this adds a dominant artificial fluctuation (roughly corresponding to the statistical error for a S/N of 100) to parameter estimation.

Since our search template family possesses a family of approximate reduction curves, it will be generally possible to estimate efficiently only three independent target observables, and four only for very high S/N. Our hope is then to find three target-parameter-estimators pairs that satisfy all three criteria, and four pairs that satisfy the consistency and robustness criteria.

It is straightforward to see that using M_s to estimate M and η_s to estimate η (or in shorthand, $M_s \rightarrow M$ and $\eta_s \rightarrow \eta$) satisfies the consistency and robustness criteria. We shall pay a special attention to the estimation of chirp mass according to $\mathcal{M}_s \equiv M_s \eta_s^{3/5} \rightarrow \mathcal{M} \equiv M \eta^{3/5}$, which satisfies all three criteria (in particular, chirp mass is conserved very accurately along reduction curves). In upper part of Table III we characterize the distribution of estimation error for M , η , and \mathcal{M} , for the same systems (with fixed masses and random local parameters)

		$(6+3)M_\odot$ (500 points)	$(9+3)M_\odot$ (500 points)	$(12+3)M_\odot$ (100 points)	$(10+10)M_\odot$ (500 points)	$(15+10)M_\odot$ (100 points)	$(15+15)M_\odot$ (100 points)
M	$(\overline{M}_s - M)/M$	+0.0232	+0.0021	-0.0066	-0.0351	-0.0206	-0.0579
	$\Delta M_s/M$	0.0817	0.0755	0.0631	0.0437	0.0603	0.0639
	1- σ /3- σ percentage	75.6%/98.0%	84.0%/97.4%	79.0%/97.0%	76.4%/98.6%	70.0%/99.0%	72.0%/100.0%
η	$\overline{\eta}_s - \eta$	-0.0057	+0.0022	+0.0038	+0.0191	+0.0122	+0.0362
	$\Delta \eta_s$	0.0268	0.0254	0.0178	0.0219	0.0283	0.0387
	1- σ /3- σ percentage	72.6%/99.0%	84.4%/98.8%	81.0%/98.0%	76.6%/98.6%	74.0%/99.0%	74.0%/100.0%
\mathcal{M}	$(\overline{\mathcal{M}}_s - \mathcal{M})/\mathcal{M}$	-0.0004	+0.0015	+0.0021	+0.0055	+0.0033	+0.0142
	$\Delta \mathcal{M}_s/\mathcal{M}$	0.0074	0.0106	0.0104	0.0092	0.0145	0.0192
	1- σ /3- σ percentage	71.6%/99.0%	69.6%/99.2%	66.0%/100.0%	71.2%/99.2%	70.0%/98.0%	80.0%/99.0%
$\frac{\mathbf{S}_{\text{eff}} \cdot \hat{\mathbf{L}}_N}{M^2}$	$\overline{\left(\frac{\hat{\mathbf{L}}_N \cdot \mathbf{S}_{\text{eff}}}{M^2}\right)_s} - \frac{\hat{\mathbf{L}}_N \cdot \mathbf{S}_{\text{eff}}}{M^2}$	+0.0236	+0.0210	+0.0129	-0.0071	-0.0015	+0.0004
	$\Delta \left[\left(\frac{\hat{\mathbf{L}}_N \cdot \mathbf{S}_{\text{eff}}}{M^2}\right)_s - \frac{\hat{\mathbf{L}}_N \cdot \mathbf{S}_{\text{eff}}}{M^2} \right]$	0.1290	0.1130	0.1010	0.0747	0.0886	0.0917
	1- σ /3- σ percentage	79.4%/98.0%	73.4%/98.8%	68.0%/100.0%	75.8%/99.0%	66.0%/100.0%	73.0%/98.0%
$\frac{\mathbf{S}_{\text{eff}}}{M}$	$\frac{1}{M} \left[\left(\frac{\mathbf{S}_{\text{eff}}}{M}\right)_s - \frac{\mathbf{S}_{\text{eff}}}{M} \right]$	+0.0253	-0.0264	-0.0183	+0.0375	+0.0028	+0.0387
	$\frac{1}{M} \Delta \left[\left(\frac{\mathbf{S}_{\text{eff}}}{M}\right)_s - \frac{\mathbf{S}_{\text{eff}}}{M} \right]$	0.1920	0.1480	0.1050	0.1170	0.1860	0.1460
	1- σ /3- σ percentage	75.0%/98.6%	72.6%/98.6%	67.0%/99.0%	75.0%/98.8%	74.0%/100.0%	79.0%/99.0%
χ_{tot}	$\overline{(\chi_{\text{tot}})_s} - \chi_{\text{tot}}$	+0.0627	-0.0053	-0.0140	+0.0174	+0.0036	+0.0149
	$\Delta [(\chi_{\text{tot}})_s - \chi_{\text{tot}}]$	0.2040	0.1610	0.1190	0.0901	0.1450	0.1220
	1- σ /3- σ percentage	81.6%/98.2%	81.8%/97.8%	85.0%/97.0%	78.8%/98.0%	71.0%/99.0%	80.0%/98.0%

TABLE III: Systematic biases, rms deviations, and percentage of samples within ± 1 and 3 deviations of the average, for six target-observable-estimator pairs. The mass configurations are those studied in Sec. IIIB.

used in Sec. IIIB to compute FFs. Each section shows the estimation bias (defined as the average of the error, and measuring a systematic displacement between observables and estimators that can in principle be removed), its rms deviation (measuring the intrinsic uncertainty in the estimation), and the percentage of estimators enclosed within 1-deviation and 3-deviation intervals (measuring the normality of the distribution). The chirp mass, which satisfies all three criteria, is indeed estimated with higher relative accuracy than both M and η . Even after statistical errors are taken into account, this accuracy should be retained for \mathcal{M} better than for M and η . The distributions of M_s , η_s , and \mathcal{M}_s are also histogrammed in Fig. 6, for $(m_1 + m_2) = (6+3)M_\odot$ and $(10+10)M_\odot$ binaries.

It is very hard to identify additional target-parameter-estimator pairs that satisfy all three criteria, mainly because double-spin binaries lack conserved quantities that clearly dominate the waveforms; so the two additional target observables that can be estimated efficiently may not have simple physical meanings. When spin-spin effects are negligible, the only truly conserved quantity that could be interesting for our purposes is $\mathbf{S}_{\text{eff}} \cdot \hat{\mathbf{L}}_N$,

with

$$\mathbf{S}_{\text{eff}} \equiv \left(1 + \frac{3m_2}{4m_1}\right) \mathbf{S}_1 + \left(1 + \frac{3m_1}{4m_2}\right) \mathbf{S}_2. \quad (27)$$

[The magnitudes of the individual spins do not satisfy the consistency criterion, since single-spin binaries (e.g., with m_1 spinning) require $|\mathbf{S}_{1s}| \rightarrow |\mathbf{S}_1|$, while double-spin, equal-mass binaries require $|\mathbf{S}_{1s}| \rightarrow |\mathbf{S}_1 + \mathbf{S}_2|$.] Therefore, we choose the target observable $\mathbf{S}_{\text{eff}} \cdot \hat{\mathbf{L}}_N/M^2$, which is conserved and closely related to the opening angle between \mathbf{S}_{eff} and $\hat{\mathbf{L}}_N$, and hence to the depth of the modulation caused by orbital precession. The estimator is naturally

$$\left[\frac{\mathbf{S}_{\text{eff}} \cdot \hat{\mathbf{L}}_N}{M^2} \right]_s \equiv \left(1 + \frac{3m_{2s}}{4m_{1s}}\right) \frac{m_{1s}^2}{M_s^2} \chi_{1s\kappa_{1s}}, \quad (28)$$

where $(m_{1,2})_s \equiv \text{Re} [(1 \pm \sqrt{1 - 4\eta_s})/2] M_s$ (taking the real part becomes necessary when $\eta_s > 0.25$). As we see from Table III, this observable can be estimated with bias within $[-0.01, +0.02]$, and with rms deviation 0.07–0.13. Although conserved, this observable is not quite constant along reduction curves. In the left

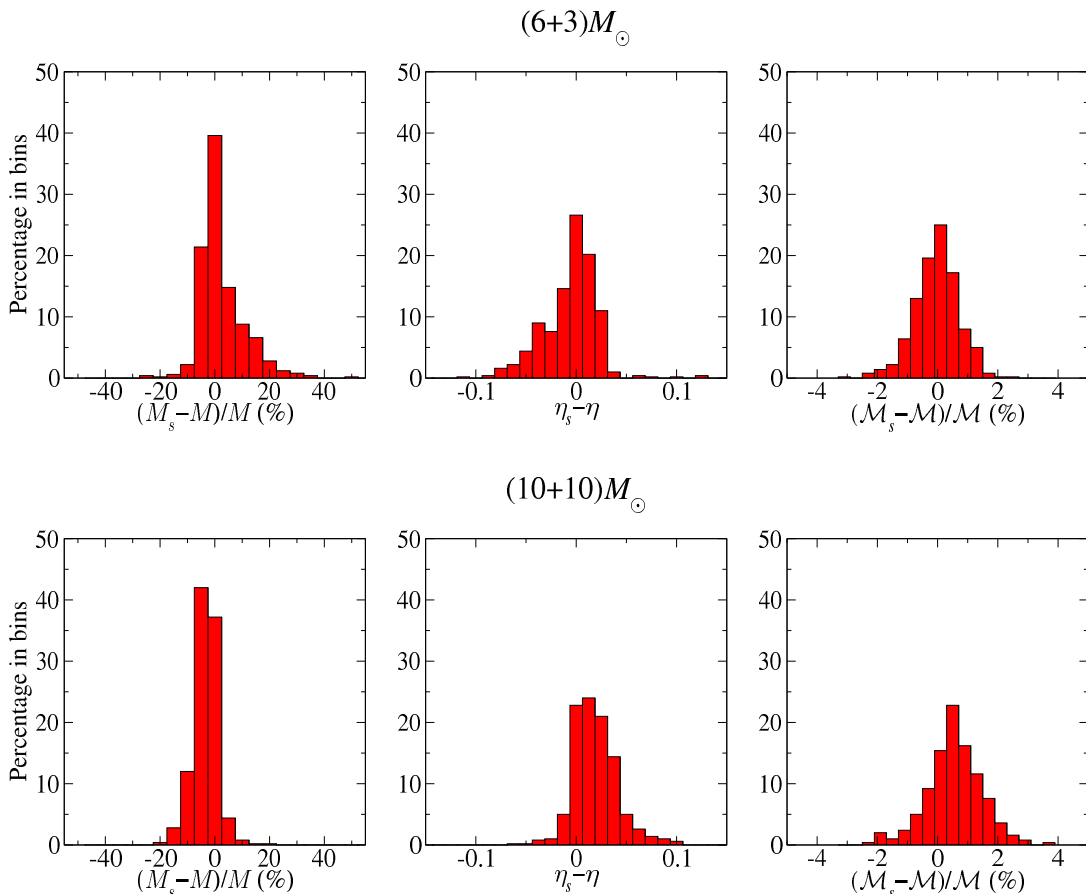


FIG. 6: Distribution of errors for the target observables M , η , and \mathcal{M} , as estimated by M_s , η_s and \mathcal{M}_s , for 500 double-spin binaries with $(m_1 + m_2) = (6 + 3)M_\odot$ and $(10 + 10)M_\odot$, maximal spins, and uniform distributions of local parameters. The \mathcal{M}_s distribution has the smallest bias and dispersion; the M_s and η_s distributions have much larger dispersion and are skewed in opposite directions (as needed to reduce the dispersion of $\mathcal{M}_s \equiv M_s \eta_s^{3/5}$).

panels of Fig. 7, we plot the distribution of the pairs $(\mathbf{S}_{\text{eff}} \cdot \hat{\mathbf{L}}_N / M^2, [\mathbf{S}_{\text{eff}} \cdot \hat{\mathbf{L}}_N / M^2]_s)$ for $(m_1 + m_2) = (6 + 3)M_\odot$ and $(10 + 10)M_\odot$ binaries. In each case we conclude that the target observable and the estimator are strongly correlated; however, the dispersion is noticeably smaller for $(10 + 10)M_\odot$ than for $(6 + 3)M_\odot$ binaries; this must be because for equal-mass binaries only spin-spin effects can cause differences between double-spin and single-spin waveforms.

In the light of Eq. (10), we choose the third target observable as $|\mathbf{S}_{\text{eff}}|/M$, which measures the instantaneous angular precession frequency divided by ω^2 . This quantity is conserved only for single-spin binaries and for equal-mass binaries with negligible spin-spin effects, so it does not completely satisfy the robustness criterion. In our study, we use the value of $|\mathbf{S}_{\text{eff}}|/M$ at the initial frequency (40 or 60 Hz) from which the equations of motion are integrated. [However, it would be more reasonable to evaluate it at the frequency at which the detector is most sensitive, or to weight its values at different frequencies according to the detector noise spectrum.] The estimator

is

$$\left[\frac{|\mathbf{S}_{\text{eff}}|}{M} \right]_s = \left(1 + \frac{3m_{2s}}{4m_{1s}} \right) \frac{m_{1s}^2}{M_s} \chi_{1s}. \quad (29)$$

To make the observable and the estimator dimensionless, we divide both by M ; Table III then shows that $|\mathbf{S}_{\text{eff}}|/M^2$ can be estimated with bias within $[-0.03, +0.04]$, and rms deviation 0.11–0.19. Despite the apparent physical meaning of $[|\mathbf{S}_{\text{eff}}|/M]_s$, this observable is also not conserved well along reduction curves. Thus, we might as well use a more familiar target observable, $\chi_{\text{tot}} \equiv \mathbf{S}_{\text{tot}}/M_s^2$, as estimated by $[\chi_{\text{tot}}]_s = \chi_{1s} m_{1s}^2 / M^2$. This pair satisfies the consistency criterion, and it changes through the inspiral at a level similar to $\mathbf{S}_{\text{eff}}/M^2$. Table III shows that χ_{tot} can be estimated with bias within $[-0.005, +0.06]$, and rms deviation 0.10–0.20. In the center and right panels of Fig. 7, we plot (target, estimator) distributions for these two spin observables, again for $(m_1 + m_2) = (6 + 3)M_\odot$ and $(10 + 10)M_\odot$ binaries. It is clear from the plots that the accuracy of estimation is poorer than for $\mathbf{S}_{\text{eff}} \cdot \hat{\mathbf{L}}_N / M^2 \rightarrow [\mathbf{S}_{\text{eff}} \cdot \hat{\mathbf{L}}_N / M^2]_s$; again,

the dispersion is smaller for the $(10+10)M_{\odot}$ binaries. For $(6+3)M_{\odot}$ binaries, the worse accuracy can be attributed in part to the fact that these two target observables are not as well conserved as $\mathbf{S}_{\text{eff}} \cdot \hat{\mathbf{L}}_N/M^2$ during evolution.

VI. CONCLUSIONS

As originally pointed out by ACST [18], the dynamics of double-spin precessing binaries become equivalent to the dynamics of single-spin binaries (at least for the purpose of computing gravitational waveforms at the leading mass-quadrupole order) in two limits: equal masses, when spin-spin effects can be neglected (then $\mathbf{S}_1 \rightarrow \mathbf{S}_{\text{tot}}$), and very different masses (then \mathbf{S}_1 tends to the spin of the heavier body). Building on this observation, on the results of Refs. [10, 21, 25], and on the (justified) assumption that spin-spin effects contribute mildly to the PN binding energy and GW flux of the binary for mass configurations of interest to ground-based GW interferometers, we conjectured that single-spin templates (as defined in Sec. III B) can be used effectually to search for double-spin precessing binaries with such masses.

We tested our conjecture by evaluating the FF between the single-spin and double-spin families, and we found confirmation in the very high FF values [see Table I and Fig. 1] for equal-mass binaries of both low and high total masses. FFs were high also for unequal-mass binaries, except for few initial spin configurations. As discussed in Sec. III D, for those configurations the evolution of the opening angles between $\hat{\mathbf{J}}$ and $\hat{\mathbf{L}}_N$ and between $\hat{\mathbf{J}}$ and $\hat{\mathbf{S}}_{1,2}$ seem to contain large oscillations, induced by spin-spin and non-equal-mass effects, that cannot be reproduced sufficiently well by single-spin systems.

The region in the single-spin parameter space needed to match double-spin binaries with $(m_1, m_2) = [3, 15]M_{\odot} \times [3, 15]M_{\odot}$ is shown in Fig. 2. Using the LIGO-I design sensitivity, we counted (very roughly) as $\sim 320,000$ the number of templates required to yield a minimum match of 0.97. The number of BCV2 templates needed for a similar mass range is somewhat larger. More generally, with respect to the detection template families introduced in Refs. [20, 21, 22, 23, 25], the advantage of the quasi-physical single-spin family suggested in this paper is the possibility of estimating the parameters of the source. In Sec. V we computed the systematic errors that would affect the measurement: the total mass M could be estimated with a fractional bias within $[-6\%, +3\%]$ and a fractional rms deviation of 5%–8%; the symmetric mass ratio η could be estimated with a bias within $[-0.06, +0.04]$ and an rms deviation of 0.02–0.04; the chirp mass \mathcal{M} could be estimated with a fractional bias within $[-0.04\%, +0.01\%]$ and a fractional rms deviation of 0.7%–2%. We also proposed estimators for certain

spin parameters of the double-spin system. For example, the parameter $(\mathbf{S}_{\text{eff}} \cdot \hat{\mathbf{L}}_N)/M^2$ [where \mathbf{S}_{eff} is defined by Eq. (28)], which is conserved when spin-spin effects can be neglected, could be estimated with a bias within $[-0.01, +0.03]$ and an rms deviation of 0.07–0.13; the parameter $\chi_{\text{tot}} \equiv \mathbf{S}_{\text{tot}}/M^2$ could be estimated with a bias within $[-0.005, +0.06]$ and an rms deviation of 0.10–0.20. However, since the mismatch metric has small components along the directions of these spin estimators, we expect that (at least for moderate S/N) statistical errors will always be dominant over the systematic errors discussed here. We defer the study of statistical errors to a forthcoming paper [43].

In evaluating the performance of the quasi-physical single-spin template family, we have assumed a *uniform* distributions for the initial local parameters (spin and orientation angles) of the double-spin target model. It would be interesting in the future to redo our analyses assuming more realistic nonuniform distributions derived from astrophysical considerations. The only available results for spin distributions in BH–BH binaries (unfortunately, with a single spin) and in NS–BH binaries were obtained using population-synthesis techniques [24, 44]. For the case of binaries formed in globular clusters, there is no theoretical argument to suggest any particular spin distribution.

Last, recent studies of PN spin-spin effects [45] suggest that, for binaries with comparable masses, the two BH spins may have become roughly *locked* into a fixed relative configuration by the time the GWs enter the band of good interferometer sensitivity. If these results are confirmed, they could provide preferred initial spin conditions, and by reducing the variability of GW signals, they could help to explain the good performance of our single-spin template family. We must however note that we were motivated in proposing our single-spin templates by the assumption that spin-spin effects never dominate, while for locking to occur spin-spin effects seem to be crucial [45].

Acknowledgments

The research of Y.C. and Y.P. was supported by NSF grant PHY-0099568 and NASA grant NAG5-12834. Y.C. is also supported by the David and Barbara Groce Fund at the San Diego Foundation. M.V. is grateful to the *Institut d’Astrophysique* in Paris for hospitality during the completion of this work; M.V.’s research was supported by the LISA Mission Science Office at the Jet Propulsion Laboratory, Caltech, where it was performed under contract with the National Aeronautics and Space Administration.

[1] A. Abramovici et al., *Science* **256**, 325 (1992); <http://www.ligo.caltech.edu>.

[2] B. Caron et al., *Class. Quantum Grav.* **14**, 1461 (1997);

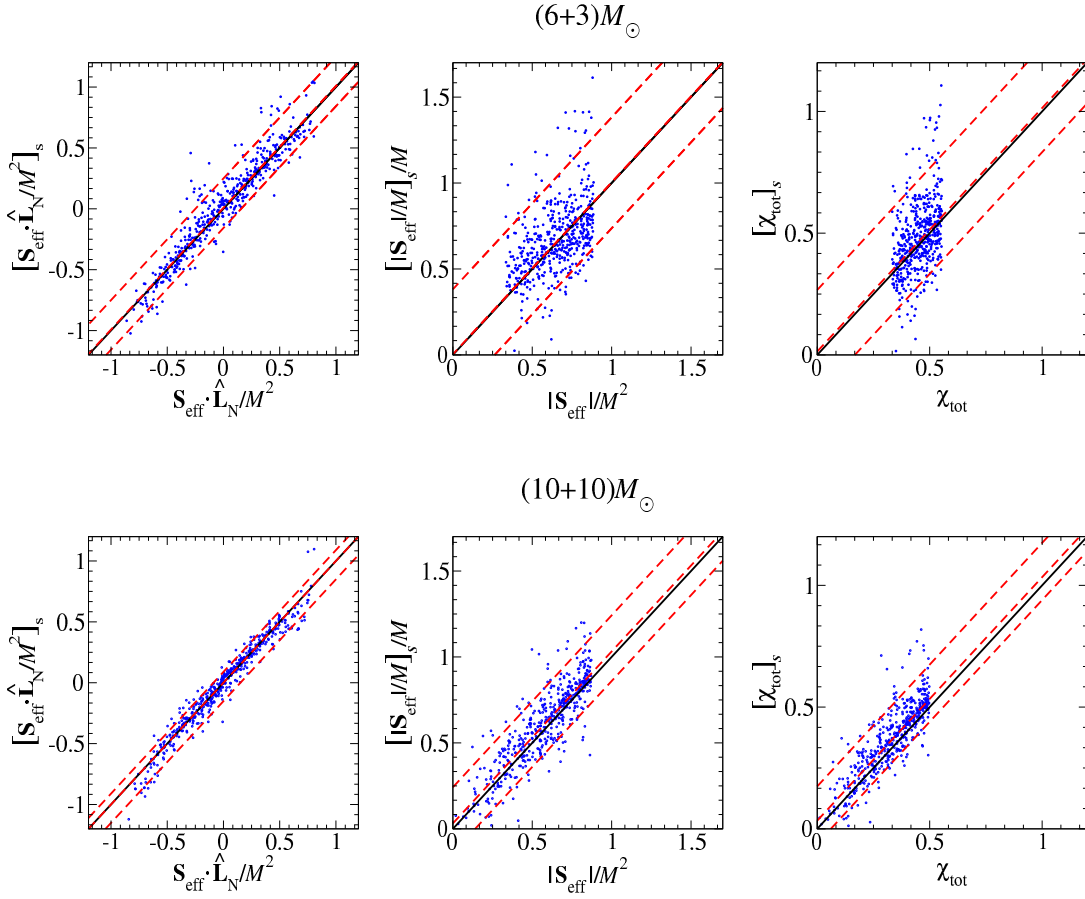


FIG. 7: Estimation of spin-related parameters for 500 double-spin binaries with $(m_1 + m_2) = (6 + 3)M_\odot$ and $(10 + 10)M_\odot$, maximal spins, and uniform distributions of local parameters. The three columns display the correlations between the (target-observable, estimator) pairs $(\mathbf{S}_{\text{eff}} \cdot \hat{\mathbf{L}}_N / M^2, [\mathbf{S}_{\text{eff}} \cdot \hat{\mathbf{L}}_N / M^2]_s)$, $(|\mathbf{S}_{\text{eff}}| / M^2, [|\mathbf{S}_{\text{eff}}| / M^2]_s / M)$, and $(\chi_{\text{tot}}, [\chi_{\text{tot}}]_s)$. In each panel, three dashed lines are used to indicate the median of the bias and the 90% percentiles above and below it. The solid line marks the line of zero bias. Lower biases correspond to solid lines closer to the central dashed lines; lower dispersions correspond to closer outer dashed lines.

- <http://www.virgo.infn.it>.
- [3] H. Lück et al., *Class. Quantum Grav.* **14**, 1471 (1997); <http://www.geo600.uni-hannover.de>.
- [4] M. Ando et al., *Phys. Rev. Lett.* **86**, 3950 (2001); <http://tamago.mtk.nao.ac.jp>.
- [5] B. Abbott et al., *Nucl. Instr. Meth. in Phys. Res. A*, **517**, 154 (2004).
- [6] B. Abbott et al., *Phys. Rev. D* **69**, 122001 (2004); **69**, 082004 (2004); **69**, 102001 (2004); **69**, 122004 (2004).
- [7] M. Burgay et al., *Nature* **426**, 531 (2003).
- [8] L. Blanchet, T. Damour, B. R. Iyer, C. M. Will, and A. G. Wiseman, *Phys. Rev. Lett.* **74**, 3515 (1995); L. Blanchet, T. Damour, and B. R. Iyer, *Phys. Rev. D* **51**, 5360 (1995); erratum, **54**, 1860 (1996); C. M. Will and A. G. Wiseman, *Phys. Rev. D* **54**, 4813 (1996).
- [9] L. E. Kidder, C. M. Will, and A. G. Wiseman, *Phys. Rev. D* **47**, 4183(R) (1993).
- [10] L. E. Kidder, *Phys. Rev. D* **52**, 821 (1995).
- [11] P. Jaranowski and G. Schäfer, *Phys. Rev. D* **57**, 7274 (1998); *ibid.* **60**, 124003 (1999); T. Damour, P. Jaranowski, and G. Schäfer, *Phys. Rev. D* **62**, 044024 (2000); *ibid.*, 021501(R) (2000); **63**, 044021 (2001).
- [12] T. Damour, P. Jaranowski, and G. Schäfer, *Phys. Lett. B* **513**, 147 (2001).
- [13] L. Blanchet, G. Faye, B. R. Iyer, B. Joguet, *Phys. Rev. D* **65**, 061501 (2002).
- [14] Y. Itoh and T. Futamase, *Phys. Rev. D* **68**, 121501 (2003); Y. Itoh, *ibid.*, **69**, 064018 (2004).
- [15] L. Blanchet, T. Damour, and G. Esposito-Farese, *Phys. Rev. D* **69**, 124007 (2004).
- [16] T. Damour, B. R. Iyer, and B. S. Sathyaprakash, *Phys. Rev. D* **63**, 044023 (2001); *Phys. Rev. D* **66**, 027502 (2002).
- [17] A. Buonanno, Y. Chen, and M. Vallisneri, *Phys. Rev. D* **67**, 024016 (2003).
- [18] T. A. Apostolatos, C. Cutler, G. J. Sussman, and K.S. Thorne, *Phys. Rev. D* **49**, 6274 (1994).
- [19] T. A. Apostolatos, *Phys. Rev. D* **52**, 605 (1995).
- [20] T. A. Apostolatos, *Phys. Rev. D* **54**, 2421 (1996).
- [21] T. A. Apostolatos, *Phys. Rev. D* **54**, 2438 (1996).
- [22] P. Grandclément, V. Kalogera, and A. Vecchio, *Phys. Rev. D* **67**, 042003 (2003).
- [23] P. Grandclément and V. Kalogera, *Phys. Rev. D* **67**, 082002 (2003).

- [24] P. Grandclément, M. Ihm, V. Kalogera, and K. Belczynski, *Phys. Rev. D* **69**, 102002 (2004).
- [25] BCV2: A. Buonanno, Y. Chen, and M. Vallisneri, *Phys. Rev. D* **67**, 104025 (2003).
- [26] Y. Pan, A. Buonanno, Y. Chen, and M. Vallisneri, *Phys. Rev. D* **69**, 104017 (2004).
- [27] In fact, such “templates” are not complete waveforms, but contain all the ingredients needed to construct the waveforms for any choice of the extrinsic parameters. Thus, they are perhaps better described as “multitemplates,” or “pseudotemplates.”
- [28] C. W. Lincoln and C. M. Will, *Phys. Rev. D* **42**, 1123 (1990); L. Wen, *Astrophys. J.* **598**, 419 (2003).
- [29] T. A. Apostolatos, *Phys. Rev. D* **52**, 605 (1995).
- [30] One example is the initial phase Φ_0 in nonspinning-binary templates: fixing all the other parameters, the value of ρ for any Φ_0 (and indeed, the maximum ρ over all Φ_0) is obtained by combining $\rho(\Phi_0 = 0)$ and $\rho(\Phi_0 = \pi/2)$.
- [31] B. S. Sathyaprakash and S. V. Dhurandhar, *Phys. Rev. D* **44**, 3819 (1991); S. V. Dhurandhar and B. S. Sathyaprakash, *ibid.*, **49**, 1707 (1994); B. S. Sathyaprakash, *ibid.*, **50**, R7111 (1994); R. Balasubramanian, B. S. Sathyaprakash, and S. V. Dhurandhar, *ibid.*, **53**, 3033 (1996); B. J. Owen, *ibid.*, 6749 (1996); B. J. Owen and B. S. Sathyaprakash, *ibid.*, **60**, 022002 (1999).
- [32] B. S. Sathyaprakash and B. F. Schutz, *Class. Quant. Grav.* **20**, S209 (2003); L. Barack and C. Cutler, *Phys. Rev. D* **69**, 082005 (2004); on the existence of reduction curves given small metric eigenvalues, C. Cutler (private communication).
- [33] To be fully consistent in using Eq. (1) up to 3.5PN order, we should include high-order spin-orbit and spin-spin terms that are not available at this time.
- [34] E. Poisson, *Phys. Rev. D* **57**, 5287 (1998).
- [35] C. Cutler and É. É. Flanagan, *Phys. Rev. D* **49**, 2658 (1994);
- [36] T. Damour, B. R. Iyer, and B. S. Sathyaprakash, *Phys. Rev. D* **57**, 885 (1998); A. Buonanno and T. Damour, *Phys. Rev. D* **59**, 084006 (1999); A. Buonanno and T. Damour, *Phys. Rev. D* **62**, 064015 (2000); T. Damour, P. Jaranowski, and G. Schäfer, *Phys. Rev. D* **62**, 084011 (2000); T. Damour, *Phys. Rev. D* **64**, 124013 (2001).
- [37] T. Damour, B. R. Iyer, P. Jaranowski, and B. S. Sathyaprakash, *Phys. Rev. D* **67**, 064028 (2003).
- [38] For double-spin binaries λ_{LS} is not constant, since the evolution of $|\mathbf{S}_{\text{tot}}|$ can lead it to oscillate [see Eq. (21)]; however, these oscillations do not destroy the qualitative picture see in Fig. 5.
- [39] When $\hat{\mathbf{L}}$ and $\hat{\mathbf{S}}_{\text{tot}}$ are almost aligned or anti-aligned, the FF is again high, since the total waveform modulation induced by orbital precession is negligible. This effect competes with nutation in determining the eventual FF, but it dominates only for a small range of θ_{LS} .
- [40] One conjecture is the following: in the single-spin case, θ_L always increases while θ_S decreases in time. In the double-spin case, oscillations are superimposed; if $\theta_{LS} > 90^\circ$, θ_L increases, and θ_S decreases (or viceversa); while if $\theta_{LS} < 90^\circ$, θ_L and θ_S either both increase or decrease in time. This difference might be the origin of the poor performance of single-spin templates $\theta_{LS} < 90^\circ$.
- [41] R. Sibson, in *Interpreting Multivariate Data*, V. Barnett, ed. (Wiley, Chichester, 1981), p. 21–36.
- [42] Qualitatively, for high-S/N events, the actual projection point lies within the template-space contour that has mismatch $\sim (S/N)^{-1}$ with the theoretical projection point.
- [43] A. Buonanno, Y. Chen, Y. Pan, and M. Vallisneri, “Gravity-wave templates for precessing binaries of spinning compact objects: III. Parameter estimation,” in preparation.
- [44] V. Kalogera, *Astrophysical Journal* **541**, 319 (2000).
- [45] J. D. Schnittman, private communication; “Spin-Orbit Resonance in Compact Binary LIGO Sources,” talk given at LSC workshop, Hanford, August 2002.